Influence of Interfacial Forces on the Hyperbolicity of the Two-Fluid Model

Michaël NDJINGA[1,2], Anela KUMBARO[1], Florian DE VUYST[2,3,4], Pascal LAURENT-GENGOUX[2,4]

1. Commissariat à l'Energie Atomique, Centre d'Etudes de Saclay, France
2. Laboratoire de Mathématiques Appliquées aux Systèmes, Ecole Centrale Paris, France
3. Centre de Mathématiques et de Leurs Applications, Ecole Normale Supérieure de Cachan, France
4. Laboratoire de Recherche Conventionné, LRC CEA-DAM/ECP, France
E-mail: michael.ndjinga@cea.fr

Abstract The Two-Fluid Model, an averaged model widely used in the modeling of two-phase compressible flows, generally fails to be hyperbolic in its basic formulation. However, interfacial forces such as the interfacial pressure term and the virtual mass force, bringing new differential terms to the system can change the previous analysis and make the problem hyperbolic. The case where the two phases are incompressible has been studied by Stuhmiller ([1]) in 1977, but till now, no proof of their efficiency in rendering the model hyperbolic exists in the compressible case. The aim of this paper is to detail the effects these forces have on the hyperbolicity of the Two-Fluid Model in the compressible case. We characterise the location and topology of the non hyperbolic regions, and propose a closure for the interfacial pressure that makes the system unconditionnally hyperbolic.

1 Introduction

The Two-Fluid Model equations have been used for more than thirty years to model two phase flows. However, they suffer the clear difficulty of not being hyperbolic in their basic formulation. This means that the mathematical problem is ill-posed in the sense of Hadamard ([2]), and numerical simulations on refined meshes show unexpected oscillations. The simplest cases, where the two phases are incompressible have been studied by Stuhmiller ([1]), who showed that additional differential terms due to the modeling of interfacial forces could make the problem hyperbolic. Interfacial pressure term and virtual mass force have been used since then to make the problem hyperbolic in the compressible cases (see Park and al. [3] and Watanabe and Kukita [4]), but no theoretical study has been made to prove and assess their efficiency. The reason is that the degree of the characteristic polynomial of the two-fluid system switches from 2 in the incompressible case to 4 in the compressible case, making it much more difficult to state when it splits over the real field.
This paper proposes to describe the locus where the two-fluid characteristic polynomial with interfacial pressure term and virtual mass force admits 4 real roots. After recalling the Two-Fluid Model basic equations in section 2, we deal in section 3 with the the problem of counting the number of real roots of a polynomial having the form given in Eq.(7). For that seek, we show that the number of real roots is the number of intersections between a given parabola (Eq.(11)) and a given hyperbola (Eq.(10)). This leads us to the geometrical problem of characterising the locus where the parabola and the hyperbola have four intersections. From that study, in section 4, we deduce the topology of the hyperbolic region of the Two-Fluid Model, which enables us to propose a model that ensures the hyperbolicity of the Two-Fluid Model with interfacial pressure term and virtual mass force.

2 The Two-Fluid Model

2.1 One dimensional equations for isentropic flows

The Two-Fluid Model equations for two-phase flow are obtained by averaging the balance equations for each separated phase, using space or time averaged quantities (see [5] and [6]). We will be considering an inviscid isentropic two-phase flow, call gas the lighter phase (subscript g), and liquid the heavier (subscript l). Assuming no mass transfer between the phases, and considering only interfacial forces, the mass and momentum balance equations for each phase can be written as follows:

$$\frac{\partial \alpha_g \rho_g}{\partial t} + \frac{\partial \alpha_g \rho_g u_g}{\partial x} = 0, \tag{1}$$

$$\frac{\partial \alpha_l \rho_l}{\partial t} + \frac{\partial \alpha_l \rho_l u_l}{\partial x} = 0, \tag{2}$$

$$\frac{\partial \alpha_g \rho_g u_g}{\partial t} + \frac{\partial \alpha_g \rho_g {u_g}^2}{\partial x} + \alpha_g \frac{\partial p}{\partial x} = F_g, \tag{3}$$

$$\frac{\partial \alpha_l \rho_l u_l}{\partial t} + \frac{\partial \alpha_l \rho_l {u_l}^2}{\partial x} + \alpha_l \frac{\partial p}{\partial x} = F_l. \tag{4}$$

With the following closure relations:

$$\alpha_g + \alpha_l = 1, \quad F_g + F_l = 0. \tag{5}$$

If we take $F_g = F_l = 0$, the system (1)-(4) can be written into the matrix form:

$$\frac{\partial U}{\partial t} + A \frac{\partial U}{\partial x} = 0,$$

with the state vector $U = \begin{pmatrix} P \\ \alpha_g \\ u_g \\ u_l \end{pmatrix}$.

It is well known that the matrix A can then have complex eigenvalues and thus system (1)-(4) is not hyperbolic. More precisely except from the very special (but important) cases when $\alpha_g = 0$, $\alpha_g = 1$ and $u_g = u_l$, the system has real eigenvalues provided:

$$(u_g - u_l)^2 \geq \frac{c_g^2 c_l^2}{\alpha_g \rho_l c_l^2 + \alpha_l \rho_g c_g^2} \left((\alpha_l \rho_g)^{\frac{1}{3}} + (\alpha_g \rho_l)^{\frac{1}{3}} \right)^3. \quad (6)$$

For most of the physical applications, $u_g \ll c_g$ and $u_l \ll c_l$, and thus the condition given in Eq.(6) is practically never satisfied. This means the system is ill-posed in the sense of Hadamard (see [2]) and numerical simulation on refined meshes show unphysical oscillations, especially around shockwaves (see for example [7]). This result generalises to the case where F_g and F_l are algebraic expression involving no derivatives of the unknowns.

However, if F_g and F_l involve derivatives of the unknowns, they bring additional terms to matrix A and can change the previous statement.

It is the case when considering the interfacial pressure term, which is a correction term due to the fact that average pressure and interfacial pressure are not exactly the same. It is modeled using the following formula:

$$F_g^p = -\triangle P \frac{\partial \alpha_g}{\partial x} = -F_l^p,$$

where $\triangle P = \left(p - p^i\right)$ is a positive parameter characterising the difference between average pressure and interfacial pressure.

We are also going to consider the virtual mass force, characterising inertial effects on an accelerated particle. We have taken the following modeling proposed by Drew and Lahey (see for example [3]):

$$\begin{aligned} F_g^{vm} &= -C_{vm} \left[\left(\frac{\partial u_g}{\partial t} + u_g \frac{\partial u_g}{\partial x} \right) - \left(\frac{\partial u_l}{\partial t} + u_l \frac{\partial u_l}{\partial x} \right) \right] \\ &= -F_l^{vm}. \end{aligned}$$

We are going to study how both the interfacial pressure term and the virtual mass force can affect the diagonalisability of matrix A by taking $F_g = F_g^p + F_g^{vm}$ and $F_l = F_l^p + F_l^{vm}$.

2.2 The key polynomial for the study of hyperbolicity

Let us introduce the following abbreviation:

$$\gamma^2 = \frac{\alpha_g \alpha_l \rho_g \rho_l}{\alpha_g \alpha_l \rho_g \rho_l + (\alpha_g \rho_g + \alpha_l \rho_l) C_{vm}} \frac{c_g^2 c_l^2}{\alpha_g \rho_l c_l^2 + \alpha_l \rho_g c_g^2}.$$

Now let λ be an eigenvalue of A, set $X = \frac{\lambda - \frac{u_g + u_l}{2}}{\gamma}$. Then, up to a constant factor, the characteristic polynomial rewrites:

$$P(X) = (X - \delta)^2 (X + \delta)^2 - K_1 (X - \delta)^2 - K_2 (X + \delta)^2 + K_3, \quad (7)$$

with

$$\begin{aligned} K_1 &= \alpha_l \rho_g + \tfrac{\alpha_g}{c_g^2} \triangle P + \tfrac{1}{\alpha_g} C_{vm}, \\ K_2 &= \alpha_g \rho_l + \tfrac{\alpha_l}{c_l^2} \triangle P + \tfrac{1}{\alpha_l} C_{vm}, \\ K_3 &= \tfrac{\triangle P}{\gamma^2}, \\ \delta &= \frac{u_g - u_l}{2\gamma}. \end{aligned}$$

System (1)-(4) is said to be strictly hyperbolic if and only if P has four distinct real roots. In this case, the matrix A is necessarily diagonalisable with real eigenvalues.

Main results

In the following sections, by a carefull analysis of the polynomial P, we are going to show the following results :

- For any value of the parameters $\alpha_g, \rho_g, \rho_l, c_g, c_l, C_{vm}$, the hyperbolic region is an unbounded and connected subset of the $(\triangle P, (u_g - u_l)^2)$ plane. It is possible from the diagram of the non hyperbolic regions (figure 15) to predict the effect a given modeling of $\triangle P$ and C_{vm} will have on the hyperbolicity of the Two-Fluid Model.

- Taking $C_{vm} = 0$, a carefull modeling of the only interfacial pressure term can indeed ensure the hyperbolicity of the Two-Fluid Model. If we are interested in small relative velocities, the critical value of $\triangle P$ is :

$$\triangle P_c = \frac{\alpha_g \alpha_l \rho_g \rho_l}{\alpha_g \rho_l + \alpha_l \rho_g} (u_g - u_l)^2.$$

A modeling with $\triangle P = (1 + \varepsilon) \triangle P_c$, $\varepsilon > 0$ will ensure hyperbolicity for a certain range of small relative velocities. The higher ε is, the larger the range is. The reason is that the double roots is nearly always convex (see Eq(19)).

- Knowing the location of the non hyperbolic regions, it is possible to correct or build closure relations for the only interfacial pressure term in order that they avoid non hyperbolic regions. In the case $C_{vm} = 0$, the simplest modeling is

$$\triangle P = \rho_g (u_g - u_l)^2.$$

which ensures hyperbolicity of the Two-Fluid Model at least for $(u_g - u_l)^2 < c_g^2$.

- Virtual mass alone has no impact on the hyperbolicity of small relative velocities.

- Coupling interfacial pressure term and virtual mass helps making the double roots curve concave and thus hyperbolicity is more easily ensured for greater velocities. The critical value for $\triangle P$ to ensure hyperbolicity of both small and large relative velocities is then given by:

$$\triangle P_c = \frac{\left(\alpha_l \rho_g + \frac{C_{vm}}{\alpha_g} \right) \left(\alpha_g \rho_l + \frac{C_{vm}}{\alpha_l} \right)}{\alpha_g \rho_l + \alpha_l \rho_g + \frac{C_{vm}}{\alpha_g \alpha_l}} (u_g - u_l)^2.$$

The critical value $\triangle P_c$ is an increasing function of C_{vm} so, the higher the virtual mass coefficient is the higher the critical value for $\triangle P$ to ensure hyperbolicity is.

In the following, we give the proof of all these assertions.

3 Mathematical analysis of the characteristic polynomial

3.1 A geometric interpretation

Let us determine when a polynomial having the form

$$P(X) = (X-\delta)^2(X+\delta)^2 - K_1(X-\delta)^2 - K_2(X+\delta)^2 + K_3, \quad (8)$$

with $K_1 \geq 0$ and $K_2 \geq 0$ admits 4 real roots.

If X is a real root of P, then calling

$$x = (X+\delta)^2, \qquad y = (X-\delta)^2, \qquad (9)$$

leads to the following relation between x and y:

$$(x-K_1)(y-K_2) = K_1K_2 - K_3. \qquad (10)$$

Note that x and y also satisfy:

$$8\delta^2(x+y) = (x-y)^2 + 16\delta^4, \qquad (11)$$
$$\text{with} \quad x \geq 0 \quad \text{and} \quad y \geq 0. \qquad (12)$$

Conversely if x and y are positive and satisfy Eq.(11) and Eq.(10), then there exists an X satisfying Eq.(9). As Eq.(10) is true, X is a root of P.

Therefore the number of real roots of P is the number of intersecting points between the parabola defined by Eq.(11) and the hyperbola defined by Eq.(10) in the $x \geq 0, y \geq 0$ quarter.

Note that if x and y satisfy Eq.(11) with $\delta \neq 0$, x and y are necessarily positive. So only in the $\delta = 0$ case should we truncate the parabola.

3.2 Description of the parabola and the hyperbola

The Parabola:

Figure 1 shows the graphic of the parabola defined by Eq.(11).

It is the 45° clockwise rotation of the parabola defined by the equation $y = \frac{1}{8\delta^2}x^2 + 2\delta^2$.

It is located on the $x \geq 0$ and $y \geq 0$ quarter and is tangent to both x and y axis at ordinate $4\delta^2$.

If $\delta = 0$ it degenerates into the $x = y$ half straight line as we should consider only the positive values of x and y.

Its base point coordinates are (δ^2, δ^2). Hence, the parabola translates along the first bisector and dilates to keep tangency to both axes with increasing values of δ.

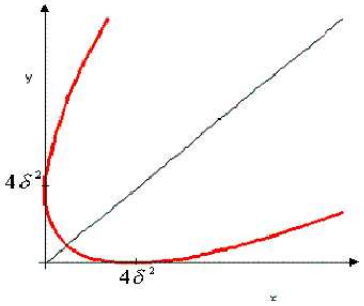

Figure 1. The parabola

The Hyperbola:

Figure 2 shows the graphic of the hyperbola defined by Eq.(10).

Its asymptotes are the $x = K_1$ and $y = K_2$ lines.

Its main parameter is $K_1K_2 - K_3$ which tells us on which side of the asymptotes it lies. Figure 3 shows an example of a four points configuration.

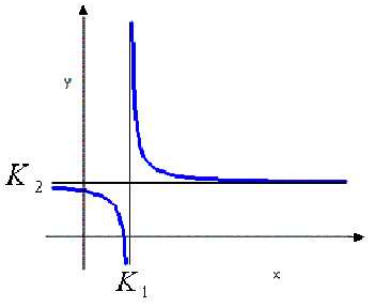

Figure 2. The hyperbola

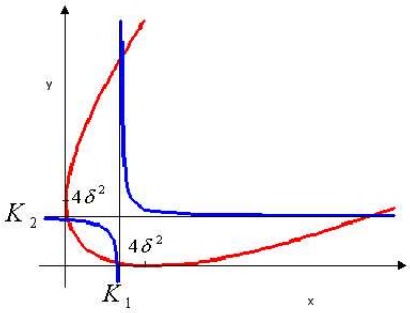

Figure 3. Hyperbolic case: four intersecting points

If we increase δ^2, we may loose two of the intersecting points as shown on figure 4.

If δ^2 goes further enough, we reach again a four intersection points configuration as shown on figure 5.

3.3 Topology of the roots regions

In the previous section, we described the respective geometries of the parabola defined by Eq.(11) and of the hyperbola defined by Eq.(10). We also proved that the number of real roots of P was the number of intersections between the parabola and the hyperbola. This means we have to study the following system with $K = K_1K_2 - K_3$:

$$\begin{cases} (x-K_1)(y-K_2) = K, \\ 8\delta^2(x+y) = (x-y)^2 + 16\delta^4. \end{cases}$$

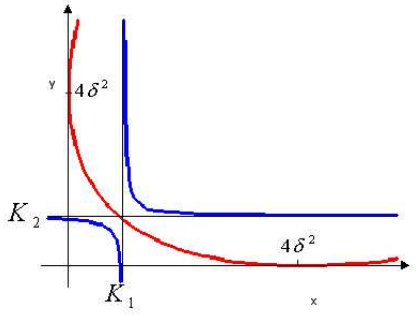

Figure 4. Non hyperbolic case: only two intersecting points

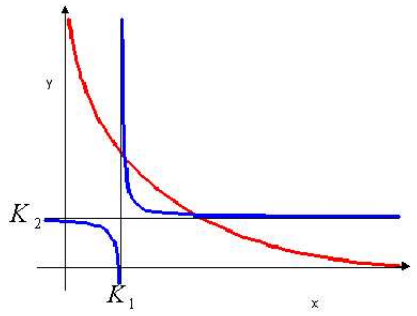

Figure 5. Hyperbolic case: again four intersecting points

Assume K_1 and K_2 are known, then the hyperbola asymptotes are fixed. The values of the two remaining parameter δ^2 and K enable us to determine the number of intersecting points between the parabola and the hyperbola. From the possible relative position of the parabola and the hyperbola, we can sketch the shape of the regions where there will be 0, 2, or 4 intersecting points as on figure 6. These regions are separated by 3 double root curves, one starting from point D, and the two other from point C.

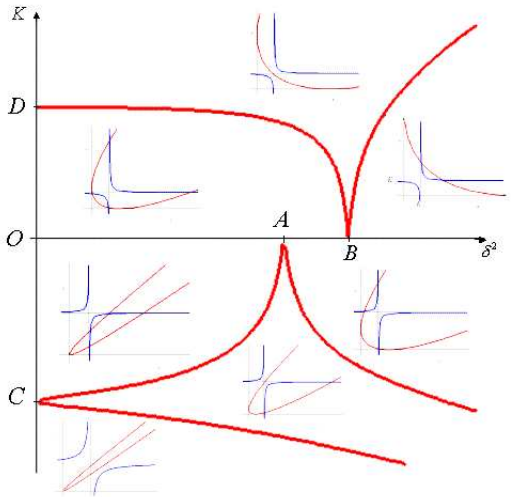

Figure 6. Sketch of confi gurations between the parabola and the hyperbole

The exact shape of the delimiting curves between the different regions depends on K_1 and K_2. Their equations can be calculated as is explained in section 6, but are very complicated. However, whatever the values for K_1 and K_2 are, the topology of the 0, 2 or 4 roots regions is the same and there are a few more invariants: the double root curves will be tangent to the x axis in 2 points A and B and join the y axis in 2 other points C and D. Each of these points corresponds to a very specific configuration enabling us to compute their coordinates.

3.4 Description of the $K = 0$ axis

On the $K = 0$ axis, the hyperbola consists of its two asymptotes. An example of the configuration on the segment $[O,A]$ is given on figure 7. On segment $[A,B]$ the configuration is that of figure 8.

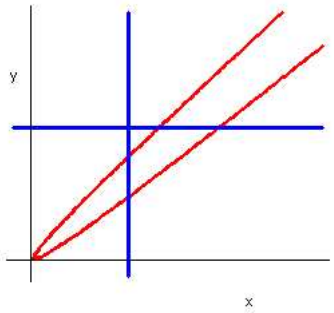

Figure 7. $K = 0$ axis: confi guration for δ^2 between O and A

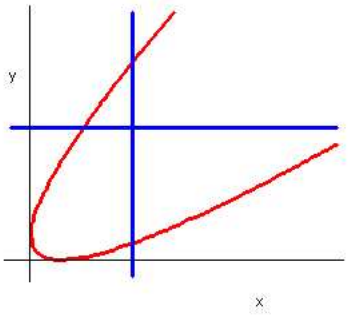

Figure 8. $K = 0$ axis: confi guration for δ^2 between A and B

Coordinates of points A and B:

Let us seek for a double root on the $K = 0$ axis. As the parabola always crosses the hyperbola four times, the only way we can get a double root is by having the parabola passing trough the hyperbola center as on figure 9.

This is equivalent to the point (K_1,K_2) being on the parabola. It corresponds to a second order polynomial in δ^2 to solve:

$$8\delta^2(K_1+K_2) = (K_1-K_2)^2 + 16\delta^4.$$

whose solutions are $\delta^2 = \left(\frac{\sqrt{K_1}-\sqrt{K_2}}{2}\right)$ and $\delta^2 = \left(\frac{\sqrt{K_1}+\sqrt{K_2}}{2}\right)$.

Hence the following (δ^2, K) coordinates for A and B:

$$A : \left(\left(\frac{\sqrt{K_1}-\sqrt{K_2}}{2}\right)^2, 0\right) \quad B : \left(\left(\frac{\sqrt{K_1}+\sqrt{K_2}}{2}\right)^2, 0\right) \tag{13}$$

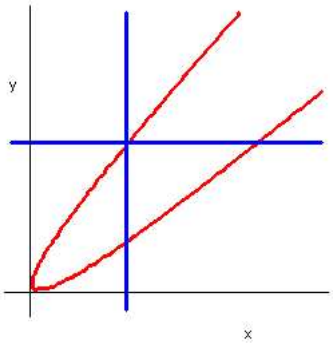

Figure 9. Configuration at point A

3.5 Description of the $\delta^2 = 0$ axis

In this case the parabola degenerates into the half line:

$$y = x, x \geq 0$$

. Figures 10 -13 show the different possible configurations for the parabola and for the hyperbola.
Segment $[-\infty, C]$ corresponds to figure 10, segment $[C, D]$ to figures 11 and 12, segment $[D, \infty]$ to figure 13.

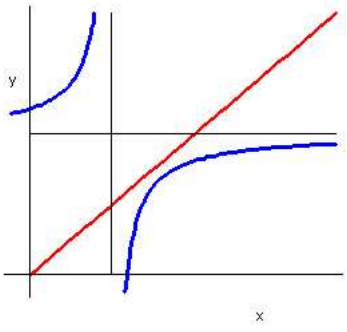

Figure 10. $\delta^2 = 0$ axis: configuration for K below C

Coordinates of points C and D:
As $\delta^2 = 0$, P is a second degree polynomial in X^2:

$$P(X) = X^4 - (K_1 + K_2)X^2 + K - K_1K_2.$$

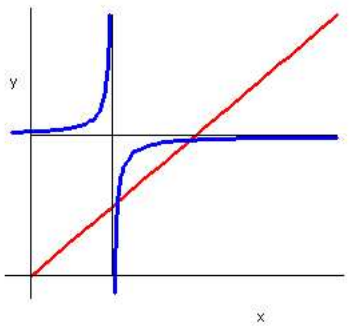

Figure 11. $\delta^2 = 0$ axis: configuration for K between C and O

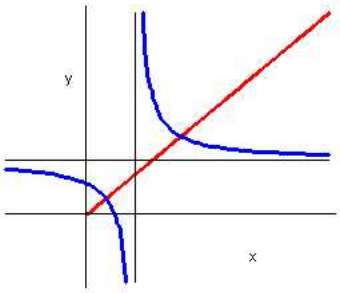

Figure 12. $\delta^2 = 0$ axis: configuration for K between O and D

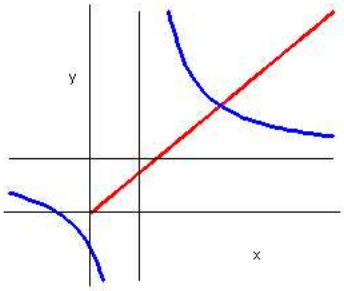

Figure 13. $\delta^2 = 0$ axis: configuration for K above D

It's fourth order discriminant is

$$\triangle = 16(K_1K_2 - K)(4K - (K_1 - K_2)^2).$$

Thus we obtain double roots when either

$$K = -\left(\frac{K_1 - K_2}{2}\right)^2 \quad \text{or} \quad K = K_1K_2.$$

Note that the last case is simply equivalent to $K_3 = 0$.

The (δ^2, K) coordinates for C and D are then the following:

$$C : (0, K_1K_2) \qquad D : \left(0, -\left(\frac{K_1 - K_2}{2}\right)^2\right) \tag{14}$$

4 Hyperbolicity analysis of isentropic flows

In the previous section, we have studied the location and topology of the hyperbolic region for a polynomial having the form:

$$P(X) = (X-\delta)^2(X+\delta)^2 - K_1(X-\delta)^2 - K_2(X+\delta)^2 + K_3.$$

In this section our aim is to deduce from the analysis in the previous section, the hyperbolicity domain when K_1, K_2, K_3 take the following forms:

$$K_1 = \alpha_l\rho_g + \frac{\alpha_g}{c_g^2}\triangle P + \frac{1}{\alpha_g}C_{vm}, \tag{15}$$

$$K_2 = \alpha_g\rho_l + \frac{\alpha_l}{c_l^2}\triangle P + \frac{1}{\alpha_l}C_{vm}, \tag{16}$$

$$K_3 = \frac{\triangle P}{\gamma^2}, \tag{17}$$

$$\delta = \frac{u_g - u_l}{2\gamma}. \tag{18}$$

4.1 Case $\triangle P = 0$ and $C_{vm} \neq 0$

Here, as $\triangle P = 0$ we have that $K_3 = 0$ and, from section 6.4, we know there will be a critical value for the relative velocity for the system (1)-(4) to be hyperbolic:

$$K_1 = \alpha_l\rho_g + \frac{1}{\alpha_g}C_{vm} > 0,$$
$$K_2 = \alpha_g\rho_l + \frac{1}{\alpha_l}C_{vm} > 0.$$

As C_{vm} should be positive, the only degenerate case is the case $\delta = 0$ which corresponds to equal velocities for both phases. Thus the system is hyperbolic if one of the two following conditions is satisfied:

$$u_g - u_l = 0,$$
$$(u_g-u_l)^2 \geq \gamma^2\left(\left(\alpha_l\rho_g + \tfrac{1}{\alpha_g}C_{vm}\right)^{\frac{1}{3}} + \left(\alpha_g\rho_l + \tfrac{1}{\alpha_l}C_{vm}\right)^{\frac{1}{3}}\right)^3.$$

And thus small relative velocities do not lead to hyperbolic systems. In absence of interfacial pressure, the virtual mass has no effect on the hyperbolicity of small relative velocities.

4.2 Case $\triangle P \neq 0$ and $C_{vm} = 0$

Description of the roots diagram

Our key parameter value has the following expression:

$$K = K_1K_2 - K_3 = \frac{\alpha_g\alpha_l}{c_g^2c_l^2}(\triangle P - \rho_g c_g^2)(\triangle P - \rho_l c_l^2).$$

We would like to deduce from the (K, δ^2) diagram on figure 6 a $(\triangle P, \delta^2)$ diagram. K equation is a parabola in the variable $\triangle P$ as shown on figure 14. As $\triangle P$ moves from 0 to infinity, K first decreases, from point D on figure 6 (as $\triangle P = 0 \Leftrightarrow K_3 = 0$)

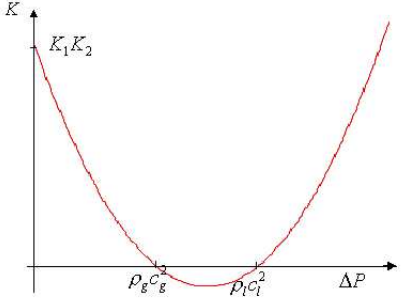

Figure 14. K describes a parabola as $\triangle P$ moves

towards its minimum at $\triangle P = \frac{\rho_g c_g^2 + \rho_l c_l^2}{2}$. As will be shown later, that minimal value is below the point C on figure 6. From that minimal value it increases to the infinity.

Throughout this process, K value cancels twice and passes twice over C. Key points A, B, and C are thus split into points $A_1, A_2, B_1, B_2, C_1, C_2$ as shown in the following $(\triangle P, \delta^2)$ roots diagram. Figure 15 shows the type of diagram we get

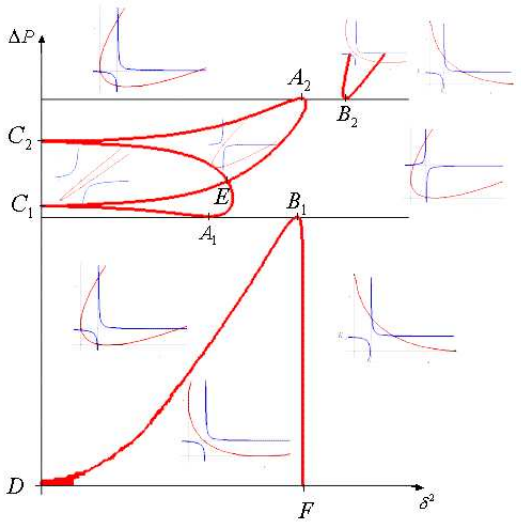

Figure 15. $\triangle P \neq 0$ and $C_{vm} = 0$: Hyperbolicity diagram

when studying the roots diagram of P. It has been drawn with logarithmic coordinates on the $\triangle P$ axis.

Point E:

From section 6 we know that the two double root curves starting from C: K_b and K_c, have respectively $-4K_1$ and $-4K_2$ as slopes at infinity. So the one with the smaller of the K_i is above. Thus if $K_1 - K_2$ changes sign while increasing $\triangle P$, the order is reversed and thus the two curves emerging from C_1 or C_2 may have to cross. This crossing is materialized by point E on the diagram. It corresponds to the case when K is negative and the two branches of the hyperbola are symmetrical through the first bisector. The parabola can be tangent to both branches at the same time as can be view in picture (16). The cross can happen

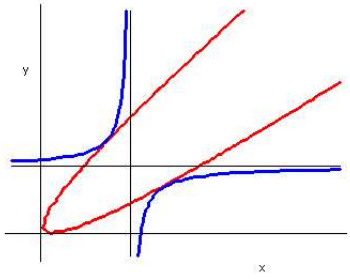

Figure 16. $C_{vm} = 0$: Confi guration at point E

for example when

$$\alpha_l \rho_g < \alpha_g \rho_l \quad \text{and} \quad \frac{\alpha_g}{c_g^2} > \frac{\alpha_l}{c_l^2}.$$

as K_1 is smaller at the beginning when $\triangle P = 0$ but moves faster than K_2 with increasing $\triangle P$. This will be the case in physical applications as $\rho_g \ll \rho_l$ and $c_g < c_l$. The last condition to be satisfied is $K \leq 0$.

Computation of A_1, A_2, B_1, B_2 coordinates:

This points correspond to the $K = 0$ case. The parameter K cancels when

$$\triangle P = \rho_g c_g^2 \quad \text{or} \quad \triangle P = \rho_l c_l^2.$$

THe values for K_1 and K_2 are then:

$$K_1 = \rho_g \quad \text{and} \quad K_2 = \frac{c_g^2}{\gamma^2} \quad \text{at points} \quad A_1 \quad \text{and} \quad B_1,$$
$$K_1 = \rho_l \quad \text{and} \quad K_2 = \frac{c_l^2}{\gamma^2} \quad \text{at points} \quad A_2 \quad \text{and} \quad B_2.$$

Thus using the formulas given in Eq.(13) we get the corresponding values for δ^2 at points A_1 and A_2, B_1 and B_2.

$$A_1 : \left(\left(\frac{c_g - \gamma\sqrt{\rho_g}}{2\gamma} \right)^2, \rho_g c_g^2 \right) \qquad A_2 : \left(\left(\frac{c_l - \gamma\sqrt{\rho_l}}{2\gamma} \right)^2, \rho_l c_l^2 \right)$$
$$B_1 : \left(\left(\frac{c_g + \gamma\sqrt{\rho_g}}{2\gamma} \right)^2, \rho_g c_g^2 \right) \qquad B_2 : \left(\left(\frac{c_l + \gamma\sqrt{\rho_l}}{2\gamma} \right)^2, \rho_l c_l^2 \right)$$

Computation of C_1, C_2 and D coordinates:

This time we have $\delta = 0$ and have to solve the equations defined by the formulas Eq.(14) at each of the points C and D to find the corresponding values for $\triangle P$.

Equation $K_1 K_2 - K_3 = \left(\frac{K_1 - K_2}{2} \right)^2$ is a second degree equation in $\triangle P$ which is equivalent to $(K_1 + K_2)^2 = 4K_3$.
Its discriminant is $16 \frac{\alpha_g \alpha_l}{c_g^2 c_l^2 \gamma^2} (\rho_l - \rho_g)(c_l^2 - c_g^2)$ and is positive if and only if $(\rho_l - \rho_g)$ and $(c_l^2 - c_g^2)$ have the same sign, which is the case in physical applications. In this case the two solutions correspond to C_1 and C_2 ordinates, which are not given here because their formulas are quite big and will not be used in the following.

Point D correspond to $K = K_1 K_2$ which is equivalent to $K_3 = 0 = \frac{\triangle P}{\gamma^2}$. Hence the coordinates for D are:

$$\boxed{\text{D: (0,0)}}$$

Computation of E and F coordinates:

Solving $K_1 = K_2$ we obtain E ordinate $\triangle P = c_g^2 c_l^2 \frac{\alpha_g \rho_l - \alpha_l \rho_g}{\alpha_g c_l^2 - \alpha_l c_g^2}$.
Then we have $K_1 = K_2 = \frac{\alpha_g{}^2 \rho_l c_l^2 - \alpha_l{}^2 \rho_g c_g^2}{\alpha_g c_l^2 - \alpha_l c_g^2}$,
and $K = -\frac{\alpha_g \alpha_l c_g^2 c_l^2}{\gamma^4} \frac{(c_g^2 - \gamma^2 \rho_g)(c_l^2 - \gamma^2 \rho_l)}{(\alpha_g c_l^2 - \alpha_l c_g^2)^2}$.
K is positive if and only if α_g is on the segment

$$I = \left[\frac{\rho_g (c_l^2 - c_g^2)}{\rho_l c_l^2 - \rho_g c_g^2}, \frac{c_g^2 (\rho_l - \rho_g)}{\rho_l c_l^2 - \rho_g c_g^2} \right]$$

.
For α_g outside I, we have a crossing point materialized by E.
From section 6 we know that $K = -4K_1 \delta^2$ and thus we get E abscissa:

$$E : \left(\frac{\alpha_g \alpha_l c_g^2 c_l^2}{4\gamma^4} \frac{(c_g^2 - \gamma^2 \rho_g)(c_l^2 - \gamma^2 \rho_l)}{(\alpha_g c_l^2 - \alpha_l c_g^2)(\alpha_g{}^2 \rho_l c_l^2 - \alpha_l{}^2 \rho_g c_g^2)}, c_g^2 c_l^2 \frac{\alpha_g \rho_l - \alpha_l \rho_g}{\alpha_g c_l^2 - \alpha_l c_g^2} \right)$$

For air-water mixtures ($\rho_g = 1 kg/m^3$, $\rho_l = 1000 kg/m^3$, $c_g = 340 m/s^2$, $c_l = 1500 m/s^2$), $I \backsimeq [10^{-7}, 5.10^{-2}]$. The crossing happens most of the time.

From section 6.4 we have

$$F : \left(\left((\alpha_g \rho_l)^{\frac{1}{3}} + (\alpha_l \rho_g)^{\frac{1}{3}} \right)^3, 0 \right)$$

Diagram for small relative velocities

Zooming on figure 15 around the origin, and setting the diagram into $\left(\triangle P, (u_g - u_l)^2 \right)$ coordinates, we get figure 17.
It has been drawn in real coordinates, with air and water numerical values: $\rho_g = 1 kg/m^3$, $\rho_l = 1000 kg/m^3$, $c_g = 340 m/s^2$, $c_l = 1500 m/s^2$ and $\alpha_g = 0.7$.

As will be shown below, the double roots curve is nearly always convex near the origin. The monotony of the OB_1 part of the double root curve is ensured by the fact that the gap between the two branches of the hyperbola vanishes as $\triangle P$ gets closer to $\rho_g c_g^2$.

Tangent line and curvature at the origin

From the Taylor expansion in Eq.(21) and using:

$$K_3 = \frac{\triangle P}{\gamma^2},$$
$$K_1 = \alpha_l \rho_g + O((u_g - u_l)^2),$$
$$K_2 = \alpha_g \rho_l + O((u_g - u_l)^2),$$

we get that the tangent line at the origin is:

$$\triangle P = \frac{\alpha_g \alpha_l \rho_g \rho_l}{\alpha_g \rho_l + \alpha_l \rho_g} (u_g - u_l)^2$$

Checking the second derivative of the double roots curve at the

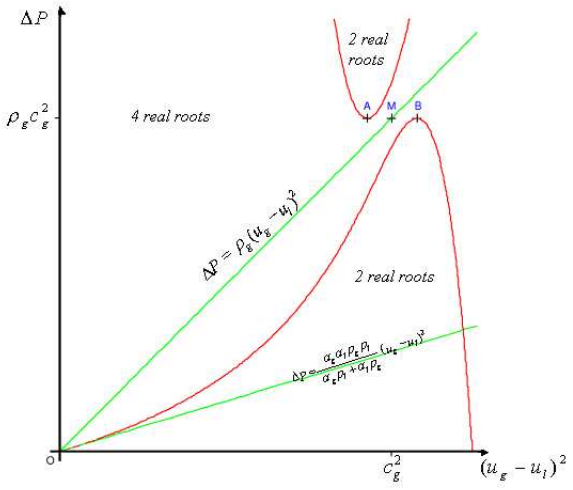

Figure 17. Hyperbolicity diagram for small relative velocities

origin using this time:

$$K_1 = \alpha_l\rho_g + \frac{\alpha_g}{c_g^2}\frac{\alpha_g\alpha_l\rho_g\rho_l}{\alpha_g\rho_l+\alpha_l\rho_g}(u_g-u_l)^2 + O((u_g-u_l)^4),$$
$$K_2 = \alpha_g\rho_l + \frac{\alpha_l}{c_l^2}\frac{\alpha_g\alpha_l\rho_g\rho_l}{\alpha_g\rho_l+\alpha_l\rho_g}(u_g-u_l)^2 + O((u_g-u_l)^4).$$

We find that the curvature at the origin is:

$$\frac{\alpha_g\alpha_l\rho_g\rho_l}{c_g^2c_l^2(\alpha_l\rho_g+\alpha_g\rho_l)^4}(\alpha_g{}^2\rho_l-\alpha_l{}^2\rho_g)(\alpha_g{}^2\rho_l{}^2c_l^2-\alpha_l{}^2\rho_g{}^2c_g^2)$$

The double roots curve is convex provided:

$$\alpha_g \geq \frac{\sqrt{\frac{\rho_g}{\rho_l}}}{1+\sqrt{\frac{\rho_g}{\rho_l}}} \quad \text{or} \quad \alpha_g \leq \frac{\frac{\rho_g c_g}{\rho_l c_l}}{1+\frac{\rho_g c_g}{\rho_l c_l}}.$$

As usually $\rho_g \ll \rho_l$ and $c_g < c_l$, the double roots curve is most of the time convex near the origin.

For example, in the case of air-water mixtures ($\rho_g = 1\,kg/m^3$, $\rho_l = 1000\,kg/m^3$, $c_g = 340\,m/s^2$, $c_l = 1500\,m/s^2$), the condition for convexity rewrites: $\alpha_g \leq 2.10^{-4}$ or $\alpha_g \geq 0.03$.

Hyperbolicity line

Now that we have located the non hyperbolic regions, we can easily predict the effect any particular modeling of the interfacial pressure has on the hyperbolicity of the Two-Fluid Model. We can also build a simple model that avoids the non hyperbolic regions. Let us find a straight line that always stays in the hyperbolic region.
The $\left((u_g-u_l)^2, \triangle P\right)$ coordinates for A_1 and B_1 are:

$$A_1\left(\left(c_g-\gamma\sqrt{\rho_g}\right)^2, \rho_g c_g^2\right) \qquad B_1\left(\left(c_g+\gamma\sqrt{\rho_g}\right)^2, \rho_g c_g^2\right)$$

Let us define M as the point with coordinates $(c_g^2, \rho_g c_g^2)$. We know from A_1 and B_1 coordinates that M is always left of B_1. The point M is right of A_1 as long as $\left(c_g-\gamma\sqrt{\rho_g}\right)^2 < c_g^2$
This is equivalent to $\alpha_g < \frac{\rho_g(c_l^2-c_g^2)}{\rho_l c_l^2-\rho_g c_g^2}$.

For air-water mixtures ($\rho_g = 1\,kg/m^3$, $\rho_l = 1000\,kg/m^3$, $c_g = 340\,m/s^2$, $c_l = 1500\,m/s^2$), the condition for M to be on $[A_1, B_1]$ rewrites:

$$\alpha_g < 2.10^{-4}.$$

Thus, because of the monotony and the convexity of the double roots curve, when $\alpha_g > 2.10^{-4}$, the (OM) line is in the hyperbolic region as long as $(u_g-u_l)^2 < c_g^2$. We actually remarked that it did not meet any non hyperbolic region even for higher relative velocities for air-water mixture numerical values. If $\alpha_g < 2.10^{-4}$, the point A_1 is left from the point M and thus, the (OM) line meets the non hyperbolic region above point A_1 which has ordinate $\rho_g c_g^2$. That means we stay in the hyperbolic region as long as $(u_g-u_l)^2 < c_g^2$. Figures 18 and 19 show the graphics of lines $(0A_1)$, (OB_1) and (OM) slopes as functions of α_g in the case of an air-water mixture.

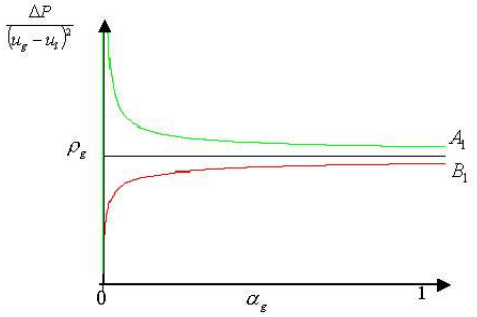

Figure 18. $\triangle P \neq 0$ and $C_{vm} = 0$: slopes of lines (OA_1), (OM) and (OB_1)

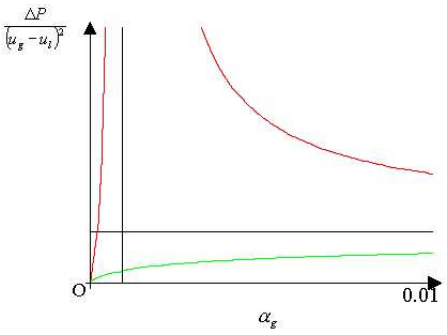

Figure 19. $\triangle P \neq 0$ and $C_{vm} = 0$: slopes of lines (OA_1), (OM) and (OB_1) for small void fractions

Thus the line $\triangle P = \rho_g(u_g-u_l)^2$ makes the problem hyperbolic for every $\alpha_g, \rho_g, \rho_l, c_g, c_l$ as long as $(u_g-u_l)^2 \leq c_g^2$.

Numerical comparisons

As can be seen from equations Eq.(15-18), as long as $\triangle P$ remains negligible compared to $\rho_g c_g^2$ and $\rho_l c_l^2$, a small perturbation of $\triangle P$ value has very little effect on the computation of

the eigenvalues and eigenvectors of the two-fluid system.
We have compared the solutions given in numerical tests by the two formulas:

$$\triangle P_1 = 1.01 \frac{\alpha_g \alpha_l \rho_g \rho_l}{\alpha_g \rho_l + \alpha_l \rho_g} (u_g - u_l)^2, \tag{19}$$

$$\triangle P_2 = \rho_g (u_g - u_l)^2. \tag{20}$$

$\triangle P_1$ is the formula introduced by D. Bestion in the industrial code CATHARE (see [8]) to obtain hyperbolicity for a certain range of small relative velocities. It is obtained by increasing the slope of the tangent line at the origin by a small factor: 1.01 . Note we have no control on the maximum relative velocity allowed in order to stay in the hyperbolic region.
$\triangle P_2$ is the formula we have seen in the previous section that guarantees hyperbolicity at as long as $(u_g - u_l)^2 \leq c_g^2$.

To compare the results obtained with these two formulas, we have chosen the Ransom faucet problem with an air and water mixture at ambient pressure. The faucet has length $L = 12\,m$ and initial and boundary conditions are:
At inlet: $\alpha_g = 0.2$, $u_g = 0\,m/s$, $u_l = 10\,m/s$.
At outlet: $P = 10^5\,Pa$.
The initial data is an uniform field with the following parameter values: $\alpha_g = 0.2$, $u_g = 0\,m/s$, $u_l = 10\,m/s$, $P = 10^5\,Pa$.

Below are the solutions obtained at time $t = 1.2s$. The results are the same.

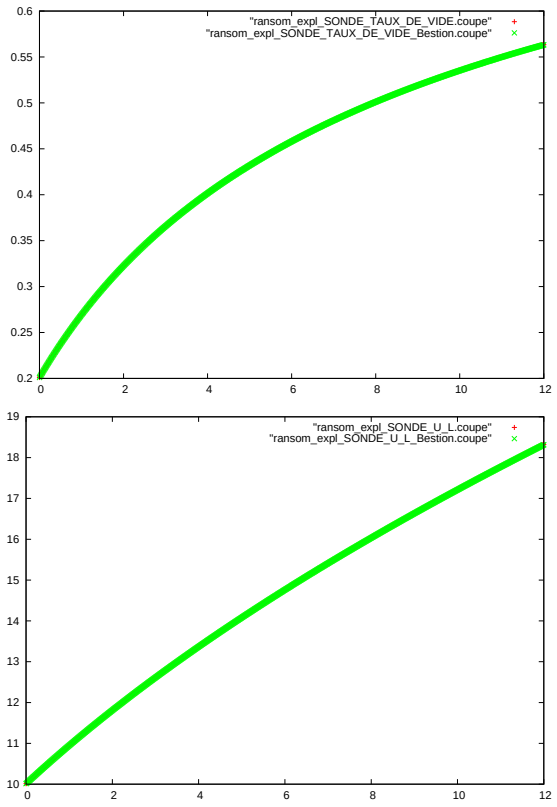

Figure 20. Void fraction and liquid velocity

4.3 Case $\triangle P \neq 0$ and $C_{vm} \neq 0$

Description of the roots diagram

The analysis is exactly the same as that of the previous section, but the formula are a litle more complicate. The expression of our key parameter is:

$$K = \frac{\alpha_g \alpha_l}{c_g^2 c_l^2} \left(\triangle P - \rho_g c_g^2 \left(1 + \frac{C_{vm}}{\alpha_g \alpha_l \rho_l} \right) \right) \times \left(\triangle P - \rho_l c_l^2 \left(1 + \frac{C_{vm}}{\alpha_g \alpha_l \rho_g} \right) \right).$$

Assume C_{vm} value is known. We would like to deduce from the (K, δ^2) diagram on figure 6 a $(\triangle P, \delta^2)$ diagram. As in the previous section, K equation is a parabola in variable $\triangle P$ cancelling twice. The topology of the roots regions will be the same as that of figure 15, with a splitting of points A, B, and C into points A_1, A_2, B_1, B_2, C_1, C_2.

Computation of the key points

We can compute the key points coordinates, using K_1, K_2, K_3, K expressions in terms of $\triangle P$ and C_{vm}, following exactly the same steps as in the previous subsection. These coordinates are complicate expressions and will not be given here.

Diagram for small relative velocities

We have shown on figure 21, the $\left(\triangle P, (u_g - u_l)^2\right)$ hyperbolicity diagram with $C_{vm} = \frac{1}{2}\alpha_g \alpha_l (\alpha_g \rho_g + \alpha_l \rho_l)$ (case of spherical bubbles).
It has been drawn with the same air and water numerical values as on figure 17: $\rho_g = 1\,kg/m^3$, $\rho_l = 1000\,kg/m^3$, $c_g = 340\,m/s^2$, $c_l = 1500\,m/s^2$ and $\alpha_g = 0.7$.

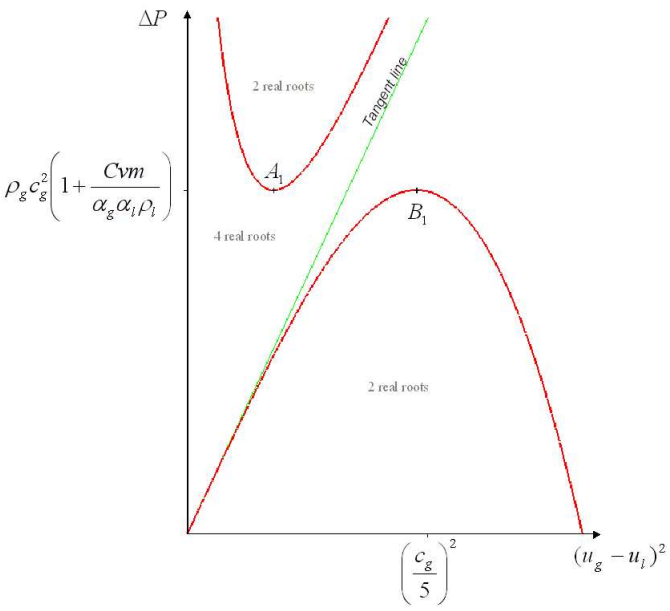

Figure 21. Hyperbolicity diagram for small relative velocities

The topology is the same as that of figure 21, but this time the double roots curve is most of the time concave near the origin.

Tangent line and curvature at the origin

As in the previous subsection, we can get that the tangent line at the origin is:

$$\boxed{\triangle P = \frac{\left(\alpha_l\rho_g+\frac{C_{vm}}{\alpha_g}\right)\left(\alpha_g\rho_l+\frac{C_{vm}}{\alpha_l}\right)}{\alpha_g\rho_l+\alpha_l\rho_g+\frac{C_{vm}}{\alpha_g\alpha_l}}(u_g-u_l)^2}$$

The slope of the tangent line is an increasing function of C_{vm}. Thus, the more virtual mass we add to the system, the more we increase the slope of the tangent line at the origin, which is the minimal slope for a line to stay in the hyperbolic region.

As in the previous subsection we can check the second derivative of the double roots curve at the origin and find:

$$\begin{aligned}\triangle P = &\frac{\left(\alpha_l\rho_g+\frac{C_{vm}}{\alpha_g}\right)\left(\alpha_g\rho_l+\frac{C_{vm}}{\alpha_l}\right)}{\alpha_g\rho_l+\alpha_l\rho_g+\frac{C_{vm}}{\alpha_g\alpha_l}}(u_g-u_l)^2+\\ &\frac{\left(\alpha_l\rho_g+\frac{C_{vm}}{\alpha_g}\right)\left(\alpha_g\rho_l+\frac{C_{vm}}{\alpha_l}\right)}{c_g^2c_l^2\left(\alpha_g\rho_l+\alpha_l\rho_g+\frac{C_{vm}}{\alpha_g\alpha_l}\right)^4}\times\\ &\left(\alpha_g\rho_lc_l^2\left(\alpha_g\rho_l+\frac{C_{vm}}{\alpha_l}\right)-\alpha_l\rho_gc_g^2\left(\alpha_l\rho_g+\frac{C_{vm}}{\alpha_g}\right)\right)\\ &\left(\frac{1}{\rho_l}\left(\alpha_g\rho_l+\frac{C_{vm}}{\alpha_l}\right)^2-\frac{1}{\rho_g}\left(\alpha_l\rho_g+\frac{C_{vm}}{\alpha_g}\right)^2\right)(u_g-u_l)^4\\ &+O(u_g-u_l)^6.\end{aligned}$$

Thus the sign of the curvature at the origin is given by:

$$\boxed{\begin{array}{c}\left(\alpha_g\rho_lc_l^2\left(\alpha_g\rho_l+\frac{C_{vm}}{\alpha_l}\right)-\alpha_l\rho_gc_g^2\left(\alpha_l\rho_g+\frac{C_{vm}}{\alpha_g}\right)\right)\times\\ \left(\frac{1}{\rho_l}\left(\alpha_g\rho_l+\frac{C_{vm}}{\alpha_l}\right)^2-\frac{1}{\rho_g}\left(\alpha_l\rho_g+\frac{C_{vm}}{\alpha_g}\right)^2\right)\end{array}}$$

Figure 22 is the plot of the curvature function with $C_{vm}=\frac{1}{2}\alpha_g\alpha_l(\alpha_g\rho_g+\alpha_l\rho_l)$.

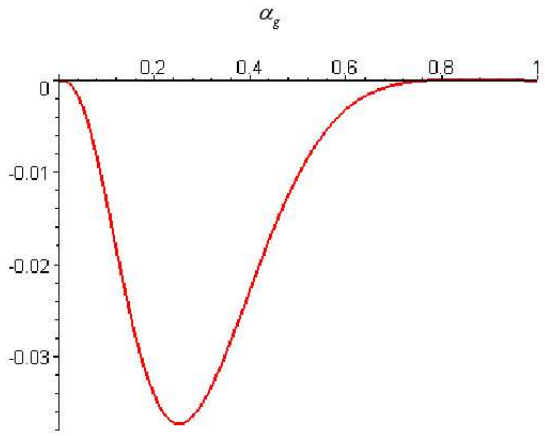

Figure 22. Curvature with $C_{vm}=\frac{1}{2}\alpha_g\alpha_l(\alpha_g\rho_g+\alpha_l\rho_l)$

5 Conclusion

We have characterised the respective effects of interfacial pressure term and virtual mass force on the hyperbolicity of the Two-Fluid Model. It appears that enough interfacial pressure indeed ensure hyperbolicity for small relatives velocity (as for example with the formula given in equation Eq.(19)), while with the formula given in Eq.(20) hyperbolicity is ensured even for a much larger range of velocities. Virtual mass force alone has no impact on the hyperbolicity of small relatives velocities. However, coupled with the interfacial pressure term, virtual mass force helps making he double roots curve concave and thus hyperbolicity is more easily ensured for greater velocities.
The tools developped here can be applied to study the impact of other differential terms (as for example turbulent dispersion, or the case $F_g \neq F_l$) on the hyperbolicity of the Two-Fluid Model, or to study model that are derived from the Two-Fluid Model, as long as the characteristic polynomial of the system takes the form given in Eq.(7).

6 Appendix: Algebraic expressions

6.1 Existence of the 3 double roots curves

Writing the polynomial $P(X)$ in the form

$$(X-\delta)^2(X+\delta)^2-K_1(X-\delta)^2-K_2(X+\delta)^2+K_1K_2-K.$$

its discriminant $\triangle$ turns out to be a third degree polynomial in K. We can solve explicitly the equation $\triangle=0$ which always admits 3 real roots K_a, K_b and K_c . Algebraic expressions can then be found for the 3 double roots curves K_a, K_b and K_c depending on δ^2, K_1, K_2 with $K_a \geq K_b \geq K_c$. Unfortunately as they are complicated, the formulas are of little help and are not given here.

Proof K_a, K_b and K_c are real

Here is the expression for $\triangle$:

$$\begin{aligned}\triangle = &-256K^3+(-256\delta^2(\delta^2-(K_1-K_2)-128(K_1-K_2)^2)K^2\\ &+(832\delta^2K_2^2K_1-6656\delta^4K_2K_1-16K_2^4+1024K_1\delta^6\\ &-16K_1^4-352K_1^2K_2^2+192K_1^3\delta^2-768K_1^2\delta^4+192K_2^3K_1\\ &+192K_1^3K_2+1024\delta^6K_2+832\delta^2K_2K_1^2+192\delta^2K_2^3-768\delta^4K_2^2)K\\ &-256\delta^2K_2^4K_1-64K_1^4K_2^2+16K_2^5K_1+16K_1^5K_2+96K_1^3K_2^3\\ &+256\delta^2K_2^3K_1^2+4096\delta^8K_2K_1-4096\delta^6K_2K_1^2-4096\delta^6K_2^2K_1\\ &+256\delta^2K_2^2K_1^3+1536\delta^4K_2K_1^3-64K_1^2K_2^4\\ &+1536\delta^4K_2^3K_1-256K_1^4K_2\delta^2+1024\delta^4K_2^2K_1^2.\end{aligned}$$

$\triangle$ is a third degree polynomial in K which admits 3 roots. To prove its 3 roots are real, we need to show that its discriminant is positive:

$$\begin{aligned}16777216\ \delta^2\ &(K_1-K_2)^2(16\delta^6+24\delta^4(K_1+K_2)\\ &-\ \delta^2(-15(K_1^2+K_2^2)+78K_1K_2)+2(K_1+K_2)^3)\geq 0.\end{aligned}$$

As the first three factors are positive, let us consider the last factor :

$$\triangle'(\delta^2)=\ 16\delta^6+24\delta^4(K_1+K_2)$$

$$+2(K_1+K_2)^3.$$

Now $\triangle^{'}$ is a third degree polynomial in δ^2. It's own discriminant $\triangle^{''}$ turns out to be always negative.

$$\triangle^{''} = -5038848K_1K_2(K_1-K_2)^4.$$

Thus there is only one real value of δ^2 that cancels the last factor of $\triangle^{'}$ with a change of sign.
As $\triangle'(0) \geq 0$ and because $\lim_{\delta^2\to-\infty}\triangle' = -\infty$, that value is negative. Thus, for real δ, $\triangle'$ never cancels, and as $\lim_{\delta\to\infty}\triangle' = +\infty$, we have that $\triangle' \geq 0$.
Hence $\triangle = 0$ admits three real roots in K wathever the values for δ, K_1 and K_2.

6.2 Taylor expansions

The algebraic expressions for K_a, K_b and K_c are very complicate. However, they give the Taylor expansions of K_a, K_b and K_c for small values of δ^2:

$$K_a = K_1K_2 - 4\frac{K_1K_2}{K_1+K_2}\delta^2 + 16\frac{K_1^2K_2^2}{(K_1+K_2)^4}\delta^4 + O(\delta^6), \quad (21)$$

$$K_b = -(\frac{K_1-K_2}{2})^2 - \sqrt{2(K_1+K_2)}(K_1-K_2)\delta + O(\delta^2), \quad (22)$$

$$K_c = -(\frac{K_1-K_2}{2})^2 + \sqrt{2(K_1+K_2)}(K_1-K_2)\delta + O(\delta^2). \quad (23)$$

And thus K_a represents the curve starting at point D on figure 6 with a slope value of $-4\frac{K_1K_2}{K_1+K_2}$ and a second derivative value of $16\frac{K_1^2K_2^2}{(K_1+K_2)^4}$.
K_b and K_c are the curves starting at point C on figure 6 with a vertical tangent.

We can also get the Taylor expansions of K_a, K_b and K_c at $\delta = \infty$:

$$\begin{array}{lcl} K_a & \sim & \delta^4, \\ K_b & \sim & -4K_1\delta^2, \\ K_c & \sim & -4K_2\delta^2. \end{array} \quad (24)$$

6.3 Case $K_1 = K_2$

In this case, K_a, K_b and K_c formulas simplify to:

$$K_a = \delta^4 - 2K_1\delta^2 + K_1^2,$$
$$K_b = K_c = -4K_1\delta^2.$$

6.4 Case $K_3 = 0$

Considering the hyperbola and the parabola defined by Eq.(10-11), $K_3 = 0$ corresponds to the case when the hyperbola passes through the origin. We see from figures 23 and 24 that δ then admits a critical value below which there are only 2 real roots and above which there are 4 real roots

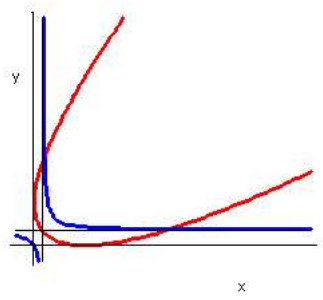

Figure 23. $K_3 = 0$: δ below critical value

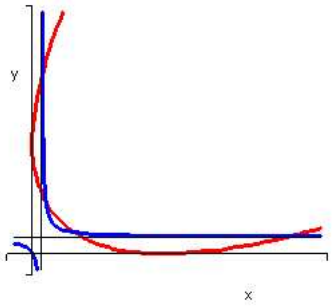

Figure 24. $K_3 = 0$: δ above critical value

Computation of the critical value
As $K_3 = 0$, the polynomial P rewrites:

$$(X-\delta)^2(X+\delta)^2 - K_1(X-\delta)^2 - K_2(X+\delta)^2$$

As it is well known (see for example [7]) P admits 4 real roots if and only if one of the following conditions is satisfied:

$K_1 = 0$, $K_2 = 0$, or $\delta = 0$.
$4\delta^2 \geq \left(K_1^{\frac{1}{3}} + K_2^{\frac{1}{3}}\right)^3$.

NOMENCLATURE

c_g	=	Gas sound speed, m/s
c_l	=	Liquid sound speed, m/s
F_g	=	Forces applied from the liquid to the gas, $kg\,m/s^2$
F_l	=	Forces applied from the gaz to the liquid, $kg\,m/s^2$
p	=	Pressure, Pa
p^i	=	Interfacial pressure, Pa
u_g	=	Convection speed of the gas, m/s
u_l	=	Convection speed of the liquid, m/s
α_g	=	Gas volume fraction, $dimensionless$
α_l	=	Liquid volume fraction, $dimensionless$
ρ_g	=	Gas density, kg/m^3
ρ_l	=	Liquid density, kg/m^3

REFERENCES

[1] J.H. Stuhmiller, The Influence of Interfacial Pressure Forces on the Character of Two-Phase Flow Model Equations, Int. J. Multiphase Flow, vol. 3, pp. 551-560, 1977.

[2] J. Hadamard, Lectures on Cauchy's Problem in Linear Par-

tial Differential Equations, Yale Univ. Press, New Haven, Conn., 1923.
[3] J.-W. Park, D.A. Drew and R.T. Lahey, Jr. The Analysis of Void Wave Propagation in Adiabatic Monodispersed Bubbly Two-Phase Flows Using an Ensemble-Averaged Two-Fluid Model, Int. J. Multiphase Flow, vol. 24, pp. 1205-1244, 1999.
[4] T. Watanabe and Y. Kukita, The Effect of The Virtual Mass Term on The Stability of The Two-Fluid Model against Perturbations, Nuclear Engineering and Design, vol. 135, pp. 327-340, 1992.
[5] M. Ishii, Thermo-Fluid Dynamic Theory of Two-Phase Flow, Eyrolles, Paris, 1975.
[6] D.A. Drew and S.L. Passman, Theory of Multicomponent Fluids, Springer-Verlag, New York, 1999.
[7] H.B. Stewart and B. Wendroff, Two-Phase Flow: Models and Methods, J. of Comp. Physics, vol. 56, pp. 363-409, 1984.
[8] D. Bestion, The Physical Closure Laws in The CATHARE Code, Nuclear Engineering and Design, vol. 124, pp. 229-245, 1990